AIAA JOURNAL
Vol. 47, No. 3, March 2009

# Flexural Stiffness Control of Multilayered Beams

Gabriel Murray and Farhan Gandhi*
*Pennsylvania State University, University Park, Pennsylvania 16802*
and
Sang-Guk Kang
*Korea Advanced Institute of Science and Technology, Daejeon 305-701, Republic of Korea*

DOI: 10.2514/1.41424

**This paper focuses on the ability to introduce change in the flexural bending stiffness of a multilayered beam. The multilayered beam comprises a base layer with polymer layers on the upper and lower surfaces and stiff cover layers. The flexural stiffness can be reduced by effecting a reduction in the shear modulus of the polymer layers by heating through glass transition. Stiffer polymer layers strongly couple the cover layers to the base beam and the entire multilayered beam bends more as an integral unit. On heating, a reduction in the shear modulus of the polymer layer results in its undergoing shear deformation as the base beam undergoes flexural bending and results in the cover layers decoupling from the base beam. This reduces the overall flexural bending stiffness. A finite element analysis is developed for the multilayered beam, and after experimentally verifying its ability to predict change in flexural bending deflection under load with a change in the polymer-layer shear modulus, it is used to conduct parametric studies. The results of the parametric studies provide broad insights into how the achievable change in flexural bending stiffness with a change in the polymer-layer modulus varies with design parameters such as the modulus and thickness of both the cover layers and the polymer layers. Changes in flexural bending stiffness by a factor of over 70 for a clamped–free beam and by a factor of over 130 for a pinned–pinned beam were observed for certain configuration designs.**

## Nomenclature

| | | |
|---|---|---|
| $b$ | = | beam width |
| $E$ | = | elastic modulus |
| $E_b$ | = | base-beam cover layer |
| $E_c$ | = | cover-layer elastic modulus |
| $E_p$ | = | polymer elastic modulus |
| $\mathbf{F}_{\mathrm{G}}$ | = | external load vector |
| $F_{\mathrm{midpoint}}$ | = | midpoint force for a pinned–pinned beam |
| $F_{\mathrm{tip}}$ | = | tip force for a clamped–free beam |
| $G$ | = | polymer-layer shear modulus |
| $K_G$ | = | global stiffness matrix |
| $k_{\mathrm{eq}}$ | = | effective flexural stiffness |
| $\ell$ | = | beam length |
| $\mathbf{q}$ | = | nodal displacement vector |
| $\mathbf{q}_G$ | = | global displacement vector |
| $t_b$ | = | base-beam thickness |
| $t_c$ | = | cover-layer thickness |
| $t_p$ | = | polymer-layer thickness |
| $u^b$ | = | base-beam axial displacement |
| $u^{\mathrm{cb}}$ | = | bottom cover-layer axial displacement |
| $u^{\mathrm{ct}}$ | = | top cover-layer axial displacement |
| $u^{\mathrm{pb}}$ | = | bottom polymer-layer axial displacement |
| $u^{\mathrm{pt}}$ | = | top polymer-layer axial displacement |
| $w_{\mathrm{midpoint}}$ | = | midpoint displacement for a pinned–pinned beam |
| $w_{\mathrm{tip}}$ | = | tip displacement for a clamped–free beam |
| $\alpha_E$ | = | ratio of cover-layer to base-beam elastic modulus |
| $\alpha_t$ | = | ratio of cover-layer to base-beam thickness |
| $\beta_G$ | = | ratio of polymer-layer shear modulus to base-beam elastic modulus |
| $\beta_t$ | = | ratio of polymer thickness to base-beam thickness |
| $\gamma$ | = | shear angle in the polymer layer |
| $\delta U$ | = | strain energy variation |
| $\partial w/\partial x$ | = | beam slope |

Received 6 October 2008; accepted for publication 30 November 2008. 

*Aerospace Engineering Department; fgandhi@engr.psu.edu (Corresponding Author).

## I. Introduction

THERE has been considerable interest in recent years in the use of variable-stiffness elements for semi-active structural control. In the early 1990s, seminal work was conducted in Japan using variable-stiffness devices for seismic response control [1,2]. These were hydraulic devices with regulator valves that effectively activated or deactivated the chevron bracing in the different stories of a building to minimize the seismic response. In [3], a semi-active variable-stiffness device was proposed comprising four spring and telescoping tube elements arranged in a rhombus configuration. The device stiffness changes by reconfiguring the aspect ratio of the rhombus using a control rod powered by a dc servomotor. Reference [4] reports on variables-stiffness telescoping axial truss members. When a piezoelectric actuator installed on the inside contracts, the clamp between the two telescoping elements is released and the axial stiffness goes to zero. Extension of the piezoelectric actuator clamps the elements to each other and restores the axial stiffness. The smart spring concept in [5] comprises a primary spring in the load path and a secondary active spring in parallel, connected to a piezoelectric stack actuator. On application of a voltage, the piezoelectric actuator generates a normal force against a structural sleeve and engages the secondary spring. One of the disadvantages of systems such as those in [4,5] is that they are dependent on friction.

Stiffness variation can also be implemented through the use of smart materials. For example, researchers have demonstrated stiffness change through capacitive shunting [6] and state-switching of piezoelectric materials [7,8]. Shape memory alloys undergo austenite-martensite phase transformations with change in temperature, and Young's modulus in the austenite phase can be 2–3 times greater than that in the martensite phase [9,10]. More recently, there has been a great deal of interest in shape memory polymers (SMPs), which display large reductions in modulus and high strain capability at high temperature, but they can store the strains and stiffen by orders of magnitude when cooled below the glass-transition temperature [11–13]. The stored strain can be recovered on heating the polymer. A magnetorheological elastomer is another material

that exhibits stiffness change: in this case, on application of a magnetic field [14]. However, relative to SMPs, the stiffness change is very modest.

References [15,16] examine the use of SMPs for morphing aircraft wings. Variable-stiffness elements are particularly interesting for application to morphing aircraft structures, because load-bearing aircraft structures are required to be stiff under normal operation, but such structures would require very high morphing-actuation force and power. The possibility of reducing the stiffness during morphing, accomplishing shape or form change at low actuation cost, and reverting to a high-stiffness load-bearing structure for normal operation is certainly an intriguing idea. Another interesting recent example of variable stiffness in morphing aerospace applications proposes the use of rotating spars in adaptive aeroelastic wings [17]. Reference [18] reports on laminar morphing materials using SMPs for variable connectivity between stiff elements. Along similar lines, an experimental study on multilayer beams with intermediate polymer layers for which the shear stiffness is reduced using embedded heating is reported in [19]. The reduced shear stiffness of the polymer decouples the stiff cover layers from the base beam to reduce the effective flexural bending stiffness of the multilayered beam.

Depending on the specific application, the stiffness variations required may either be *per cycle* or *quasi-static*. Semi-active systems with quasi-static stiffness/damping changes are also described as *adaptive-passive* systems. A capacitively shunted piezoelectric material can undergo rapid change in stiffness, but the magnitude of the stiffness change is relatively modest. In contrast, a shape memory polymer can undergo very large changes in stiffness, but because the stiffness change is temperature-driven, the bandwidth is expected to be quite low. Such a system, however, would be very well-suited for applications in which quasi-static, or relatively slow, variation in stiffness is required.

The current paper expands on the experimental study presented in [19]. After reviewing the underlying physical mechanism for enabling flexural stiffness variation of a multilayered beam in Sec. II, a description of the analytical model for the system developed in this study is presented in Sec. III. Next, experimental validation of the analytical results is presented in Sec. IV, followed by parametric studies in Sec. V.

## II. Description of Concept for Beam Flexural Stiffness Variation

Figure 1a shows a schematic representation of a multilayered beam with stiff (metal or composite) layers and an intermediate polymer layer. For the purpose of discussion here, the bottom layer is referred to as the base beam, and the top layer is referred to as the cover layer. When subjected to flexural bending, the deformation mode of this multilayered beam depends strongly on the shear modulus of the polymer layer, vis-à-vis the base beam and cover layer. If the shear modulus of the polymer layer is very high, the deformation is as shown in the schematic in Fig. 1b. The stiff top layer is coupled to the base beam, and all three layers contribute to the flexural bending stiffness. Thus, when the polymer layer is stiff, the multilayer beam behaves like an integral structure with a large cross-sectional depth and a correspondingly high flexural bending stiffness. On the other hand, if the shear modulus of the polymer layer is low, the multilayered beam deforms as depicted in the schematic in Fig. 1c. In this case, as the base beam undergoes flexural bending, the soft polymer layer undergoes shear and the cover layer is decoupled from the base beam. The beam no longer bends as an integral unit and its effective flexural bending stiffness is reduced. This principle is similar to that used in constrained-layer damping treatments [20–30], in which a stiff cover or constraining layer induces oscillatory shear in a viscoelastic polymer layer (and dissipates energy) as the base beam undergoes flexural oscillations. It is then clear that the overall flexural stiffness of the composite multilayered beam could be controlled if the shear modulus of the intermediate polymer layer could be varied.

The shear modulus of a typical polymer reduces significantly with an increase in temperature. Figure 2 (with data from [31]) shows this characteristic for a couple of commercially available polymers. At low temperatures, the polymer is in the glassy state and has a high shear modulus. As the temperature increases, the polymer's shear modulus rapidly decreases. At high temperatures, the polymer is in the rubbery state and its shear modulus can be several orders of magnitude lower than the glassy modulus. By varying the temperature of the polymer layer and correspondingly varying its shear modulus, the cover layer could be decoupled, to varying degrees, from the base beam or strongly coupled to the base beam. Correspondingly, the overall flexural stiffness of the multilayered beam could be varied.

## III. Analytical Model and Solution Scheme

This section describes the analytical model developed and used to study the multilayered beam. The beam comprises stiff (metal or composite) layers and intermediate polymer layers. The model is developed for a symmetric multilayered system with a central base beam, identical polymer layers attached to the top and bottom surfaces of the base beam, and identical upper and lower cover layers. A section of the beam is represented schematically in Fig. 3. The base beam and the cover layers undergo only normal strains, whereas the polymer layers also undergo shear strains. The kinematics of deformation and the strains in each layer are described in Secs. III.A and III.B, respectively. This is followed by expressions for the strain energy variation (Sec. III.C), the spatial discretization of the structure

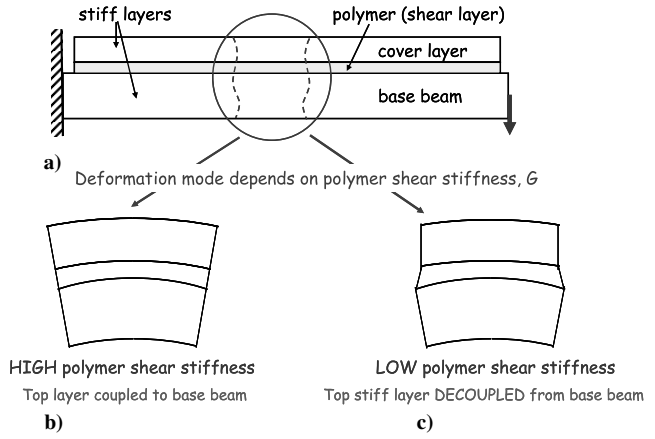


**Fig. 1 Schematic representation of a multilayered beam and deformation modes corresponding to high and low polymer shear moduli.**

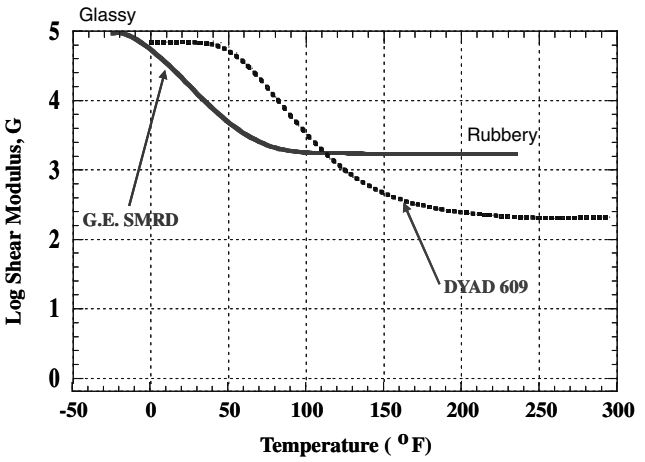


**Fig. 2 Typical variation in polymer shear modulus with increase in temperature.**

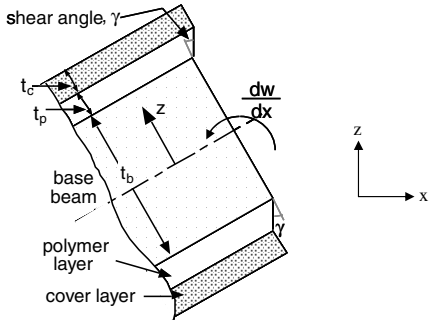


**Fig. 3 Schematic of a beam section and kinematics of deformation.**

using the finite element method (Sec. III.D), and calculation of the effective flexural stiffness (Sec. III.E).

### A. Kinematics of Deformation

Figure 3 shows a section of the beam in the deformed configuration and can be used to obtain expressions for the axial displacements in the individual layers. The axial displacement in the base beam is

$$u^b = -z\frac{\partial w}{\partial x} \tag{1}$$

Axial displacements in the top and bottom polymer layers, respectively, are

$$u^{\mathrm{pt}} = -z\frac{\partial w}{\partial x} + \left(z - \frac{t_b}{2}\right)\gamma \quad \text{and} \quad u^{\mathrm{pb}} = -z\frac{\partial w}{\partial x} + \left(z + \frac{t_b}{2}\right)\gamma \tag{2}$$

and the axial displacements in the top and bottom cover layers, respectively, are

$$u^{\mathrm{ct}} = -z\frac{\partial w}{\partial x} + t_p\gamma \quad \text{and} \quad u^{\mathrm{cb}} = -z\frac{\partial w}{\partial x} - t_p\gamma \tag{3}$$

### B. Strains in the Individual Layers

The normal strains in the individual layers can then be obtained by simply differentiating Eqs. (1–3) with respect to $x$. These are available in [20–22]. The transverse shear strain $\varepsilon_{zx}$ is zero for the base beam and the cover layers. For both upper and lower polymer layers, $\varepsilon_{zx} = \gamma$.

### C. Strain Energy Variation

The strain energy variation with contributions due to flexural and shear deformations can be written as

$$\begin{aligned}\delta U &= \int_{\text{volume}} (\delta\varepsilon_{xx}\sigma_{xx} + \delta\varepsilon_{xz}\sigma_{xz})\mathrm{d}V \\ &= \int_0^L \left\{ \int_{\text{cross section}} \delta\varepsilon_{xx}E(z)\varepsilon_{xx}b\mathrm{d}z + \int_{\text{cross section}} \delta\varepsilon_{zx}G\varepsilon_{zx}b\mathrm{d}z \right\}\mathrm{d}x\end{aligned} \tag{4}$$

In Eq. (4), the polymer layers alone contribute to the shear strain energy variations. Introducing the expressions for strains in the various layers into Eq. (4) and evaluating the integrals over the cross section yields

$$\delta U = \int_0^L \begin{bmatrix} \frac{\partial^2\delta w}{\partial x^2} & \frac{\partial\delta\gamma}{\partial x} \end{bmatrix} \begin{bmatrix} C_{22} & C_{23} \\ C_{23} & C_{33} \end{bmatrix} \begin{Bmatrix} \frac{\partial^2 w}{\partial x^2} \\ \frac{\partial\gamma}{\partial x} \end{Bmatrix} \mathrm{d}x + \int_0^L \delta\gamma[2Gbt_p]\gamma\mathrm{d}x \tag{5}$$

where

$$\begin{aligned} C_{22} &= \frac{E_b b t_b^3}{12} + \frac{2E_p b}{3}\left[\left(\frac{t_b}{2}+t_p\right)^3 - \left(\frac{t_b}{2}\right)^3\right] \\ &\quad + \frac{2E_c b}{3}\left[\left(\frac{t_b}{2}+t_p+t_c\right)^3 - \left(\frac{t_b}{2}+t_p\right)^3\right] \\ C_{23} &= 2E_p b\left[-\frac{1}{3}\left\{\left(\frac{t_b}{2}+t_p\right)^3 - \left(\frac{t_b}{2}\right)^3\right\}\right. \\ &\quad \left. + \frac{t_b}{4}\left\{\left(\frac{t_b}{2}+t_p\right)^2 - \left(\frac{t_b}{2}\right)^2\right\}\right] \\ &\quad - E_c b t_p\left[\left(\frac{t_b}{2}+t_p+t_c\right)^2 - \left(\frac{t_b}{2}+t_p\right)^2\right] \\ C_{33} &= \frac{2E_p b t_p^3}{3} + 2E_c b t_p^2 t_c \end{aligned} \tag{6}$$

Note that the shear modulus and Young's modulus of the polymer layers will vary with temperature.

### D. Finite Element Discretization

The equations of motion are obtained by using the expressions for strain energy variation [Eq. (5)] with the principle of virtual work and discretizing the structure using the finite element method, as in Fig. 4. Cubic shape functions are used for the transverse displacement, and linear shape functions are used for the shear angle, as in [20–23]. The element degree-of-freedom (or nodal displacement) vector $\{\mathbf{q}\}$ is defined as

$$\{\mathbf{q}\} = \lfloor\, w_1 \quad \theta_1 \quad \gamma_1 \quad w_2 \quad \theta_2 \quad \gamma_2 \,\rfloor^T \tag{7}$$

Introducing the shape functions into Eq. (5) and integrating along the element yields the element stiffness matrix given next (this process is presented in greater detail in [20–23]):

$$K = \begin{bmatrix} C_{22}(\frac{12}{l^3}) & C_{22}(-\frac{6}{l^2}) & 0 & C_{22}(-\frac{12}{l^3}) & C_{22}(-\frac{6}{l^2}) & 0 \\ & C_{22}(\frac{4}{l}) & -\frac{C_{23}}{l} & C_{22}(\frac{6}{l^2}) & C_{22}(\frac{2}{l}) & \frac{C_{23}}{l} \\ & & \frac{C_{33}}{l} + \frac{2Gbt_p l}{3} & 0 & \frac{C_{23}}{l} & -\frac{C_{33}}{l} + \frac{Gbt_p l}{3} \\ & & & C_{22}(\frac{12}{l^3}) & C_{22}(\frac{6}{l^2}) & 0 \\ & & & & C_{22}(\frac{4}{l}) & -\frac{C_{23}}{l} \\ & & & & & \frac{C_{33}}{l} + \frac{2Gbt_p l}{3} \end{bmatrix} \tag{8}$$

The element stiffness matrices can be assembled to obtain the global stiffness matrix. After application of geometric boundary conditions, the system equations of motion can then be written as

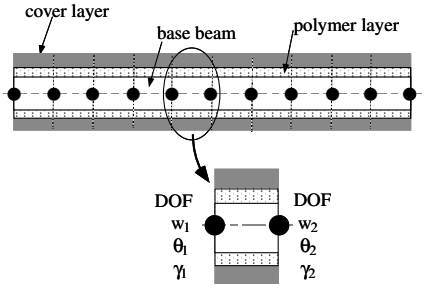


**Fig. 4 Finite element discretization of a multilayer beam (DOF denotes degrees of freedom).**

$$K_G \mathbf{q}_G = \mathbf{F}_G \tag{9}$$

### E. Calculation of the Effective Beam Flexural Stiffness

Clamped–free and pinned–pinned beams are considered in the present study. For the clamped–free beams, a static tip force is applied, and for the pinned–pinned beams, a concentrated static force is applied at the midpoint. These forces appear in the global load vector $\mathbf{F}_G$ in Eq. (9), which can be solved to obtain the beam displacements $\mathbf{q}_G$. The tip displacement of the clamped–free beam and the midpoint displacement of the pinned–pinned beam are used to calculate the effective flexural stiffness.

For the clamped–free beam,

$$K_{\text{eq}} = F_{\text{tip}}/w_{\text{tip}} \tag{10a}$$

For the pinned–pinned beam,

$$K_{\text{eq}} = F_{\text{midpoint}}/w_{\text{midpoint}} \tag{10b}$$

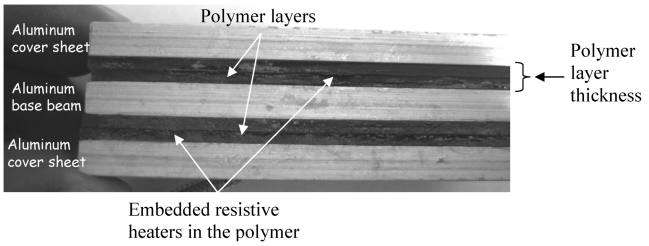


**Fig. 5 Close-up photograph of a section of a multilayered beam showing the embedded resistive heaters in the polymer layer.**

## IV. Validation of the Analysis

Reference [19] describes, in detail, experiments that were conducted to demonstrate variation in the flexural bending stiffness of the temperature-controlled multilayered beam. The experiments are described very briefly in this section, followed by a validation of the analysis. The experiment consisted of several clamped–free aluminum and polymer multilayered beams. The polymer layers were heated with embedded resistive heaters (Fig. 5). To validate the analysis, the beams' displacement under a 30 N tip load was measured as the polymer layer was heated.

The analysis presented in Sec. III is validated for three different cases. In the first and second cases, the polymer used was a cast acrylic material (polymer 1), and the thicknesses were 0.125 and 0.25 in., respectively. In the third case, the polymer used was polyvinyl chloride type I (polymer 2), and the thickness was 0.125 in. The beam length in each case was 4.5 in., and the width of all sections (base beam, polymer layers, and cover layers) was 1 in. The aluminum central base layer and the top and bottom cover layers were each 0.1875 in. thick. Figures 6a–6c show the measured and calculated beam tip deflections under a 30 N tip load as a function of increasing polymer-layer temperature. In all three figures, it is

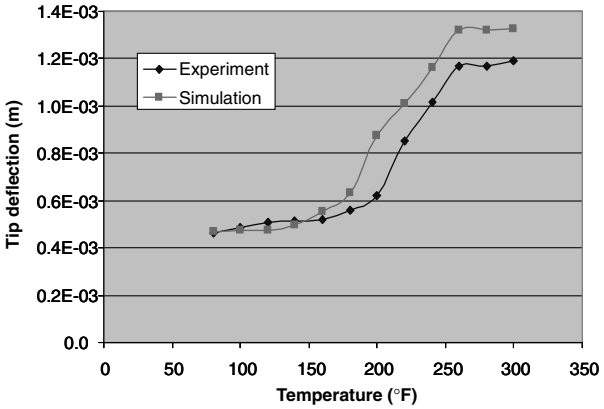


**a) Polymer 1, acrylic sheet, $t_p = 2\times0.0625$ in.**

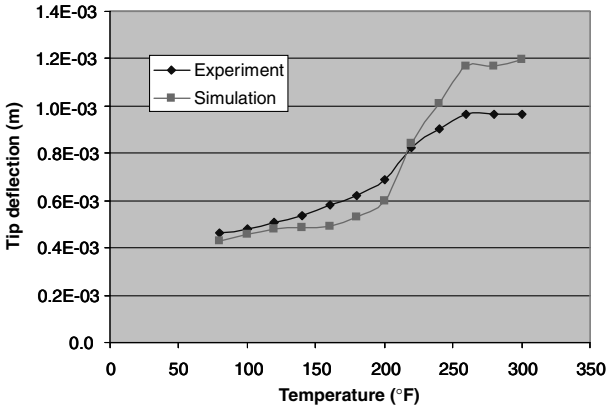


**b) Polymer 1, acrylic sheet, $t_p = 2\times0.125$ in.**

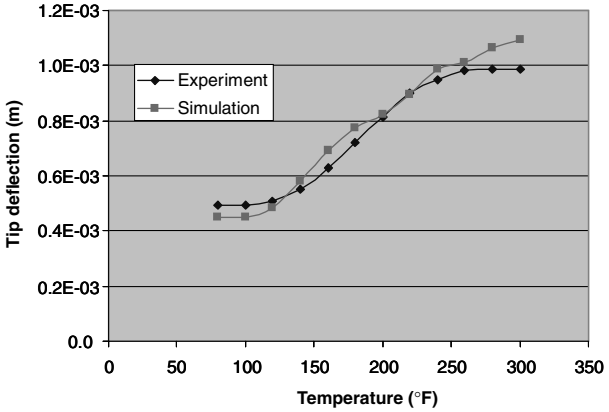


**c) Polymer 2, PVC, $t_p = 2\times0.125$ in.**

**Fig. 6 Beam tip deflection versus polymer-layer temperature under a 30 N tip load.**

**Table 1 Clamped–free beam results**

| | | | $\beta_G$ | | | | | | | | |
|---|---|---|---|---|---|---|---|---|---|---|---|
| $\alpha_E$ | $\alpha_t$ | $\beta_t$ | 1.E − 06 ($\beta_{G,\min}$) | 1.E − 05 | 1.E − 04 ($\beta_{G,\max-3}$) | 1.E − 03 ($\beta_{G,\min+3}$) | 1.E − 02 | 1.E − 01 ($\beta_{G,\max}$) | $K_{\max}/K_{\min}$ | $K_{\max}/K_{\max-3}$ | $K_{\min+3}/K_{\min}$ |
| 0.1 | 0.01 | 0.1 | 1628.8 | 1632.8 | 1634.6 | 1637.9 | 1668.4 | 1973.1 | 1.21 | 1.21 | 1.01 |
| | | 0.5 | 1631.8 | 1647.9 | 1659.2 | 1690.9 | 1982.6 | 4895.2 | 3.00 | 2.95 | 1.04 |
| | | 1 | 1636.4 | 1672.7 | 1706.7 | 1820.7 | 2885 | 13,503 | 8.25 | 7.91 | 1.11 |
| | 0.05 | 0.1 | 1642.5 | 1673.2 | 1690.2 | 1698.7 | 1730.1 | 2034.8 | 1.24 | 1.20 | 1.03 |
| | | 0.5 | 1638.1 | 1705.4 | 1781.6 | 1844.2 | 2143.9 | 5057.5 | 3.09 | 2.84 | 1.13 |
| | | 1 | 1641.6 | 1749.1 | 1935.1 | 2136.2 | 3225.1 | 13,846 | 8.43 | 7.16 | 1.30 |
| | 0.1 | 0.1 | 1650.4 | 1716.6 | 1763.3 | 1784.3 | 1818.3 | 2123.3 | 1.29 | 1.20 | 1.08 |
| | | 0.5 | 1640.7 | 1742.7 | 1914.8 | 2039.9 | 2361.4 | 5278.5 | 3.22 | 2.76 | 1.24 |
| | | 1 | 1643.8 | 1784.6 | 2145.4 | 2511.8 | 3667.5 | 14,300 | 8.70 | 6.67 | 1.53 |
| | 0.5 | 0.1 | 1725.1 | 2040.8 | 2577 | 2933.7 | 3080.2 | 3401.5 | 1.97 | 1.32 | 1.70 |
| | | 0.5 | 1692.2 | 1907.1 | 2747.5 | 3866.6 | 4811.5 | 7875.3 | 4.65 | 2.87 | 2.28 |
| | | 1 | 1692.4 | 1917.1 | 3022.5 | 5153.9 | 7926.9 | 19,042 | 11.25 | 6.30 | 3.05 |
| | 1 | 0.1 | 2055.1 | 2689.7 | 4251.7 | 5838.5 | 6558.7 | 6973.5 | 3.39 | 1.64 | 2.84 |
| | | 0.5 | 1990 | 2314.9 | 3861.6 | 6894.1 | 9977.6 | 13,719 | 6.89 | 3.55 | 3.46 |
| | | 1 | 1985.9 | 2287 | 3960.4 | 8325.5 | 15,207 | 28,229 | 14.21 | 7.13 | 4.19 |
| | 2 | 0.1 | 4452.4 | 5977.5 | 10,953 | 18,415 | 23,143 | 24,347 | 5.47 | 2.22 | 4.14 |
| | | 0.5 | 4296.5 | 4902 | 8315.3 | 17,110 | 29,449 | 37,491 | 8.73 | 4.51 | 3.98 |
| | | 1 | 4280.9 | 4769.5 | 7903.3 | 17,880 | 37,907 | 60,592 | 14.15 | 7.67 | 4.18 |
| 1 | 0.01 | 0.1 | 1646.2 | 1703.6 | 1744 | 1762.5 | 1796.1 | 2101.1 | 1.28 | 1.20 | 1.07 |
| | | 0.5 | 1638.8 | 1732.4 | 1890.5 | 2007.1 | 2325.9 | 5242.5 | 3.20 | 2.77 | 1.22 |
| | | 1 | 1642.2 | 1775.2 | 2117 | 2467.3 | 3616.5 | 14,248 | 8.68 | 6.73 | 1.50 |
| | 0.05 | 0.1 | 1656 | 1832.8 | 2129.8 | 2313.6 | 2403.6 | 2717.2 | 1.64 | 1.28 | 1.40 |
| | | 0.5 | 1642.4 | 1789.5 | 2383.5 | 3141.6 | 3843.6 | 6854 | 4.17 | 2.88 | 1.91 |
| | | 1 | 1645.3 | 1818.3 | 2699 | 4361.7 | 6650.7 | 17,628 | 10.71 | 6.53 | 2.65 |
| | 0.1 | 0.1 | 1663.5 | 1904 | 2504.3 | 3013.9 | 3257.5 | 3599.5 | 2.16 | 1.44 | 1.81 |
| | | 0.5 | 1647 | 1811.4 | 2653.2 | 4200 | 5730.4 | 9024.6 | 5.48 | 3.40 | 2.55 |
| | | 1 | 1649.4 | 1834 | 2921 | 5695.1 | 10,035 | 22,012 | 13.35 | 7.54 | 3.45 |
| | 0.5 | 0.1 | 2096.3 | 2597.7 | 4834 | 9569.4 | 14,496 | 16,213 | 7.73 | 3.35 | 4.56 |
| | | 0.5 | 2059.3 | 2303.9 | 3888.9 | 9214.7 | 21,362 | 33,344 | 16.19 | 8.57 | 4.47 |
| | | 1 | 2058.9 | 2300.6 | 3933.8 | 10,145 | 29,970 | 6.38E + 04 | 30.98 | 16.21 | 4.93 |
| | 1 | 0.1 | 4984.1 | 5881.4 | 10,694 | 23,458 | 42,548 | 50,970 | 10.23 | 4.77 | 4.71 |
| | | 0.5 | 4914.7 | 5277.8 | 7971.5 | 18,556 | 47,282 | 84,450 | 17.18 | 10.59 | 3.78 |
| | | 1 | 4910.3 | 5235.6 | 7754.6 | 18,684 | 55,723 | 1.35E + 05 | 27.45 | 17.38 | 3.81 |
| | 2 | 0.1 | 27,846 | 29,888 | 44,089 | 89,425 | 1.66E + 05 | 2.17E + 05 | 7.78 | 4.92 | 3.21 |
| | | 0.5 | 27,685 | 28,349 | 34,201 | 64,693 | 1.47E + 05 | 2.78E + 05 | 10.04 | 8.12 | 2.34 |
| | | 1 | 27,670 | 28,192 | 32,943 | 60,922 | 1.52E + 05 | 3.59E + 05 | 12.97 | 10.89 | 2.20 |
| 10 | 0.01 | 0.1 | 1655.1 | 1865.2 | 2391.6 | 2828.7 | 3040.5 | 3377.3 | 2.04 | 1.41 | 1.71 |
| | | 0.5 | 1642 | 1793.2 | 2575.5 | 4002.3 | 5411.3 | 8669.6 | 5.28 | 3.37 | 2.44 |
| | | 1 | 1644.9 | 1819.5 | 2857 | 5498.5 | 9619.3 | 21,504 | 13.07 | 7.53 | 3.34 |
| | 0.05 | 0.1 | 1663.8 | 1945 | 3275.8 | 5893.5 | 8403.2 | 9.45E + 03 | 5.68 | 2.88 | 3.54 |
| | | 0.5 | 1647.8 | 1813.8 | 2926.7 | 6674.8 | 14,829 | 2.37E + 04 | 14.38 | 8.10 | 4.05 |
| | | 1 | 1650 | 1834.2 | 3092.7 | 7897.3 | 23,118 | 5.11E + 04 | 30.97 | 16.52 | 4.79 |
| | 0.1 | 0.1 | 1695.6 | 2008.2 | 3676.5 | 8117.8 | 1.48E + 04 | 1.80E + 04 | 10.60 | 4.89 | 4.79 |
| | | 0.5 | 1677.3 | 1852.5 | 3066.8 | 7709.4 | 2.19E + 04 | 4.21E + 04 | 25.09 | 13.72 | 4.60 |
| | | 1 | 1679.3 | 1870 | 3195.4 | 8615.5 | 3.03E + 04 | 8.32E + 04 | 49.56 | 26.05 | 5.13 |
| | 0.5 | 0.1 | 5752.3 | 6327.5 | 10,351 | 25,749 | 71,627 | 1.30E + 05 | 22.52 | 12.52 | 4.48 |
| | | 0.5 | 5714.5 | 5972 | 8122.1 | 18,742 | 59,039 | 1.90E + 05 | 33.32 | 23.45 | 3.28 |
| | | 1 | 5714 | 5966.7 | 8093.7 | 18,896 | 63,513 | 2.67E + 05 | 46.66 | 32.94 | 3.31 |
| | 1 | 0.1 | 34,221 | 35,223 | 43,889 | 87,320 | 2.09E + 05 | 4.09E + 05 | 11.94 | 9.31 | 2.55 |
| | | 0.5 | 34,152 | 34,530 | 38,106 | 62,937 | 1.58E + 05 | 4.45E + 05 | 13.02 | 11.67 | 1.84 |
| | | 1 | 34,149 | 34,485 | 37,693 | 60,978 | 1.58E + 05 | 5.20E + 05 | 15.22 | 13.79 | 1.79 |
| | 2 | 0.1 | 2.62E + 05 | 2.64E + 05 | 2.84E + 05 | 4.25E + 05 | 8.73E + 05 | 1.65E + 06 | 6.29 | 5.79 | 1.62 |
| | | 0.5 | 2.62E + 05 | 2.62E + 05 | 2.69E + 05 | 3.27E + 05 | 6.27E + 05 | 1.45E + 06 | 5.54 | 5.39 | 1.25 |
| | | 1 | 2.62E + 05 | 2.62E + 05 | 2.67E + 05 | 3.15E + 05 | 5.90E + 05 | 1.49E + 06 | 5.68 | 5.56 | 1.20 |
| 100 | 0.01 | 0.1 | 1658.2 | 1931.8 | 3426 | 7343.4 | 1.31E + 04 | 1.58E + 04 | 9.53 | 4.61 | 4.43 |
| | | 0.5 | 1643.4 | 1804.5 | 2935.8 | 7279.5 | 2.03E + 04 | 3.89E + 04 | 23.69 | 13.26 | 4.43 |
| | | 1 | 1645.8 | 1826 | 3088.8 | 8269 | 2.88E + 04 | 7.91E + 04 | 48.08 | 25.62 | 5.02 |
| | 0.05 | 0.1 | 1.70E + 03 | 2.00E + 03 | 3.83E + 03 | 1.08E + 04 | 3.58E + 04 | 6.87E + 04 | 40.38 | 17.92 | 6.34 |
| | | 0.5 | 1.68E + 03 | 1.85E + 03 | 3.07E + 03 | 8.35E + 03 | 3.27E + 04 | 1.25E + 05 | 74.28 | 40.73 | 4.96 |
| | | 1 | 1.69E + 03 | 1.87E + 03 | 3.19E + 03 | 8.95E + 03 | 3.85E + 04 | 1.98E + 05 | 117.19 | 61.91 | 5.31 |
| | 0.1 | 0.1 | 1988.5 | 2315.1 | 4388.7 | 12,726 | 49,841 | 1.31E + 05 | 65.88 | 29.85 | 6.40 |
| | | 0.5 | 1969.9 | 2147.6 | 3468.8 | 9359.5 | 37,830 | 1.86E + 05 | 94.18 | 53.48 | 4.75 |
| | | 1 | 1971.7 | 2164.7 | 3577.9 | 9872.7 | 42,345 | 2.57E + 05 | 130.42 | 71.87 | 5.01 |
| | 0.5 | 0.1 | 42,300 | 42,905 | 48,563 | 85,778 | 2.27E + 05 | 6.86E + 05 | 16.22 | 14.13 | 2.03 |
| | | 0.5 | 42,263 | 42,526 | 45,081 | 65,498 | 1.61E + 05 | 5.45E + 05 | 12.90 | 12.10 | 1.55 |
| | | 1 | 42,263 | 42,521 | 45,029 | 65,232 | 1.62E + 05 | 5.84E + 05 | 13.82 | 12.97 | 1.54 |
| | 1 | 0.1 | 3.27E + 05 | 3.28E + 05 | 3.38E + 05 | 4.24E + 05 | 8.52E + 05 | 2.06E + 06 | 6.31 | 6.10 | 1.30 |
| | | 0.5 | 3.27E + 05 | 3.27E + 05 | 3.31E + 05 | 3.66E + 05 | 6.12E + 05 | 1.55E + 06 | 4.74 | 4.68 | 1.12 |
| | | 1 | 3.27E + 05 | 3.27E + 05 | 3.30E + 05 | 3.62E + 05 | 5.93E + 05 | 1.55E + 06 | 4.73 | 4.68 | 1.11 |
| | 2 | 0.1 | 2.60E + 06 | 2.60E + 06 | 2.62E + 06 | 2.83E + 06 | 4.23E + 06 | 8.70E + 06 | 3.35 | 3.32 | 1.09 |
| | | 0.5 | 2.60E + 06 | 2.60E + 06 | 2.61E + 06 | 2.67E + 06 | 3.26E + 06 | 6.25E + 06 | 2.40 | 2.40 | 1.03 |
| | | 1 | 2.60E + 06 | 2.60E + 06 | 2.61E + 06 | 2.66E + 06 | 3.13E + 06 | 5.88E + 06 | 2.26 | 2.26 | 1.02 |

**Table 2 Pinned–pinned beam results**

| | | | $\beta_G$ | | | | | | | | |
|---|---|---|---|---|---|---|---|---|---|---|---|
| $\alpha_E$ | $\alpha_t$ | $\beta_t$ | 1.E − 06 ($\beta_{G,\min}$) | 1.E − 05 | 1.E − 04 ($\beta_{G,\max-3}$) | 1.E − 03 ($\beta_{G,\min+3}$) | 1.E − 02 | 1.E − 01 ($\beta_{G,\max}$) | $K_{\max}/K_{\min}$ | $K_{\max}/K_{\max-3}$ | $K_{\min+3}/K_{\min}$ |
| 0.1 | 0.01 | 0.1 | 26,103 | 26,148 | 26,158 | 26,208 | 26,695 | 31,570 | 1.21 | 1.21 | 1.00 |
| | | 0.5 | 26,191 | 26,479 | 26,596 | 27,073 | 31,758 | 78,604 | 3.00 | 2.96 | 1.03 |
| | | 1 | 26,306 | 27,036 | 27,478 | 29,250 | 46,617 | 2.20E + 05 | 8.37 | 8.02 | 1.11 |
| | 0.05 | 0.1 | 26,438 | 26,989 | 27,129 | 27,194 | 27,683 | 32,558 | 1.23 | 1.20 | 1.03 |
| | | 0.5 | 26,361 | 27,854 | 29,017 | 29,685 | 34,392 | 81,239 | 3.08 | 2.80 | 1.13 |
| | | 1 | 26,463 | 28,971 | 32,398 | 34,934 | 52,393 | 2.26E + 05 | 8.54 | 6.98 | 1.32 |
| | 0.1 | 0.1 | 26,640 | 27,978 | 28,488 | 28,606 | 29,101 | 33,976 | 1.28 | 1.19 | 1.07 |
| | | 0.5 | 26,440 | 28,814 | 31,963 | 33,196 | 37,973 | 84,828 | 3.21 | 2.65 | 1.26 |
| | | 1 | 26,541 | 29,937 | 37,674 | 42,273 | 60,025 | 2.34E + 05 | 8.80 | 6.20 | 1.59 |
| | 0.5 | 0.1 | 28,193 | 35,977 | 46,175 | 48,762 | 49,557 | 54,464 | 1.93 | 1.18 | 1.73 |
| | | 0.5 | 27,434 | 32,822 | 54,996 | 72,220 | 79,942 | 1.27E + 05 | 4.63 | 2.31 | 2.63 |
| | | 1 | 27,464 | 33,157 | 66,048 | 1.11E + 05 | 1.39E + 05 | 3.14E + 05 | 11.43 | 4.75 | 4.04 |
| | 1 | 0.1 | 33,939 | 51,043 | 89,323 | 1.04E + 05 | 1.07E + 05 | 1.12E + 05 | 3.29 | 1.25 | 3.07 |
| | | 0.5 | 32,368 | 40,733 | 88,917 | 1.53E + 05 | 1.74E + 05 | 2.23E + 05 | 6.88 | 2.51 | 4.73 |
| | | 1 | 32,284 | 40,022 | 96,089 | 2.23E + 05 | 2.91E + 05 | 4.71E + 05 | 14.58 | 4.90 | 6.92 |
| | 2 | 0.1 | 73,594 | 1.16E + 05 | 2.69E + 05 | 3.68E + 05 | 3.85E + 05 | 3.91E + 05 | 5.32 | 1.46 | 4.99 |
| | | 0.5 | 69,793 | 85,270 | 1.97E + 05 | 4.50E + 05 | 5.55E + 05 | 6.15E + 05 | 8.81 | 3.12 | 6.45 |
| | | 1 | 69,434 | 81,782 | 1.85E + 05 | 5.55E + 05 | 8.16E + 05 | 1.03E + 06 | 14.83 | 5.57 | 7.99 |
| 1 | 0.01 | 0.1 | 26,540 | 27,700 | 28,142 | 28,250 | 28,744 | 33,620 | 1.27 | 1.19 | 1.06 |
| | | 0.5 | 26,393 | 28,568 | 31,456 | 32,625 | 37,394 | 8.42E + 04 | 3.19 | 2.68 | 1.24 |
| | | 1 | 26,503 | 29,704 | 37,008 | 41,441 | 5.92E + 04 | 2.33E + 05 | 8.79 | 6.29 | 1.56 |
| | 0.05 | 0.1 | 26,823 | 31,029 | 36,541 | 37,954 | 38,607 | 43,499 | 1.62 | 1.19 | 1.41 |
| | | 0.5 | 26,539 | 30,159 | 45,096 | 56,797 | 63,512 | 1.11E + 05 | 4.17 | 2.45 | 2.14 |
| | | 1 | 26,641 | 30,964 | 56,005 | 9.04E + 04 | 1.16E + 05 | 2.91E + 05 | 10.91 | 5.19 | 3.39 |
| | 0.1 | 0.1 | 27,016 | 32,989 | 4.64E + 04 | 5.15E + 04 | 5.27E + 04 | 5.77E + 04 | 2.13 | 1.24 | 1.91 |
| | | 0.5 | 26,657 | 30,754 | 54,470 | 8.61E + 04 | 9.86E + 04 | 1.46E + 05 | 5.49 | 2.69 | 3.23 |
| | | 1 | 26,737 | 31,386 | 65,207 | 1.42E + 05 | 1.89E + 05 | 3.67E + 05 | 13.72 | 5.63 | 5.32 |
| | 0.5 | 0.1 | 34,300 | 4.77E + 04 | 1.25E + 05 | 2.27E + 05 | 2.54E + 05 | 2.62E + 05 | 7.65 | 2.10 | 6.63 |
| | | 0.5 | 33,414 | 39,613 | 9.30E + 04 | 3.11E + 05 | 4.88E + 05 | 5.66E + 05 | 16.94 | 6.09 | 9.31 |
| | | 1 | 33,411 | 39,539 | 9.58E + 04 | 4.15E + 05 | 8.72E + 05 | 1.16E + 06 | 34.65 | 12.09 | 12.43 |
| | 1 | 0.1 | 81,193 | 1.05E + 05 | 2.74E + 05 | 6.56E + 05 | 8.08E + 05 | 8.34E + 05 | 10.27 | 3.05 | 8.08 |
| | | 0.5 | 79,531 | 88,539 | 1.72E + 05 | 6.44E + 05 | 1.29E + 06 | 1.51E + 06 | 18.94 | 8.78 | 8.10 |
| | | 1 | 79,438 | 87,482 | 1.64E + 05 | 7.11E + 05 | 1.99E + 06 | 2.67E + 06 | 33.63 | 16.26 | 8.95 |
| | 2 | 0.1 | 4.50E + 05 | 5.01E + 05 | 9.25E + 05 | 2.44E + 06 | 3.44E + 06 | 3.61E + 06 | 8.02 | 3.90 | 5.43 |
| | | 0.5 | 4.47E + 05 | 4.63E + 05 | 6.17E + 05 | 1.73E + 06 | 4.26E + 06 | 5.32E + 06 | 11.90 | 8.61 | 3.88 |
| | | 1 | 4.46E + 05 | 4.59E + 05 | 5.82E + 05 | 1.61E + 06 | 5.30E + 06 | 7.93E + 06 | 17.76 | 13.61 | 3.60 |
| 10 | 0.01 | 0.1 | 26,833 | 32,007 | 43,607 | 4.81E + 04 | 4.92E + 04 | 5.41E + 04 | 2.02 | 1.24 | 1.79 |
| | | 0.5 | 26,559 | 30,312 | 52,051 | 8.10E + 04 | 9.29E + 04 | 1.41E + 05 | 5.29 | 2.70 | 3.05 |
| | | 1 | 26,653 | 31,036 | 62,943 | 1.36E + 05 | 1.81E + 05 | 3.58E + 05 | 13.45 | 5.69 | 5.09 |
| | 0.05 | 0.1 | 27,075 | 3.43E + 04 | 7.61E + 04 | 1.32E + 05 | 1.46E + 05 | 1.53E + 05 | 5.64 | 2.01 | 4.86 |
| | | 0.5 | 26,705 | 30,874 | 6.68E + 04 | 2.14E + 05 | 3.34E + 05 | 4.02E + 05 | 15.04 | 6.01 | 8.00 |
| | | 1 | 26,766 | 31,420 | 7.42E + 04 | 3.17E + 05 | 6.68E + 05 | 9.26E + 05 | 34.61 | 12.49 | 11.85 |
| | 0.1 | 0.1 | 2.76E + 04 | 3.58E + 04 | 9.48E + 04 | 2.28E + 05 | 2.82E + 05 | 2.94E + 05 | 10.64 | 3.10 | 8.26 |
| | | 0.5 | 2.72E + 04 | 3.16E + 04 | 7.22E + 04 | 3.03E + 05 | 6.24E + 05 | 7.53E + 05 | 27.68 | 10.43 | 11.12 |
| | | 1 | 2.72E + 04 | 3.21E + 04 | 7.79E + 04 | 4.03E + 05 | 1.18E + 06 | 1.66E + 06 | 60.90 | 21.29 | 14.78 |
| | 0.5 | 0.1 | 93,243 | 1.08E + 05 | 2.41E + 05 | 9.95E + 05 | 2.04E + 06 | 2.31E + 06 | 24.76 | 9.59 | 10.68 |
| | | 0.5 | 92,342 | 98,646 | 1.60E + 05 | 6.81E + 05 | 2.84E + 06 | 4.64E + 06 | 50.30 | 28.97 | 7.37 |
| | | 1 | 92,337 | 98,521 | 1.59E + 05 | 7.07E + 05 | 3.85E + 06 | 8.48E + 06 | 91.80 | 53.15 | 7.65 |
| | 1 | 0.1 | 5.52E + 05 | 5.77E + 05 | 8.10E + 05 | 2.49E + 06 | 6.32E + 06 | 7.85E + 06 | 14.21 | 9.69 | 4.51 |
| | | 0.5 | 5.51E + 05 | 5.60E + 05 | 6.50E + 05 | 1.48E + 06 | 6.18E + 06 | 1.27E + 07 | 23.06 | 19.54 | 2.68 |
| | | 1 | 5.51E + 05 | 5.59E + 05 | 6.39E + 05 | 1.40E + 06 | 6.83E + 06 | 1.97E + 07 | 35.68 | 30.74 | 2.55 |
| | 2 | 0.1 | 4.22E + 06 | 4.27E + 06 | 4.77E + 06 | 9.02E + 06 | 2.42E + 07 | 3.42E + 07 | 8.10 | 7.16 | 2.14 |
| | | 0.5 | 4.21E + 06 | 4.23E + 06 | 4.39E + 06 | 5.94E + 06 | 1.71E + 07 | 4.24E + 07 | 10.05 | 9.65 | 1.41 |
| | | 1 | 4.22E + 06 | 4.23E + 06 | 4.35E + 06 | 5.59E + 06 | 1.58E + 07 | 5.27E + 07 | 12.51 | 12.11 | 1.33 |
| 100 | 0.01 | 0.1 | 2.70E + 04 | 3.41E + 04 | 8.53E + 04 | 2.01E + 05 | 2.47E + 05 | 2.58E + 05 | 9.57 | 3.03 | 7.45 |
| | | 0.5 | 2.66E + 04 | 3.07E + 04 | 6.79E + 04 | 2.79E + 05 | 5.74E + 05 | 6.96E + 05 | 26.11 | 10.25 | 10.48 |
| | | 1 | 2.67E + 04 | 3.13E + 04 | 7.45E + 04 | 3.81E + 05 | 1.11E + 06 | 1.58E + 06 | 59.03 | 21.15 | 14.27 |
| | 0.05 | 0.1 | 2.77E + 04 | 3.55E + 04 | 1.07E + 05 | 5.11E + 05 | 1.08E + 06 | 1.23E + 06 | 44.33 | 11.51 | 18.44 |
| | | 0.5 | 2.73E + 04 | 3.15E + 04 | 7.27E + 04 | 4.15E + 05 | 1.87E + 06 | 3.10E + 06 | 113.66 | 42.72 | 15.20 |
| | | 1 | 2.74E + 04 | 3.21E + 04 | 7.79E + 04 | 4.83E + 05 | 2.87E + 06 | 6.43E + 06 | 235.13 | 82.63 | 17.64 |
| | 0.1 | 0.1 | 32,370 | 40,852 | 1.21E + 05 | 6.87E + 05 | 2.04E + 06 | 2.59E + 06 | 79.86 | 21.38 | 21.22 |
| | | 0.5 | 31,919 | 36,368 | 79,931 | 4.66E + 05 | 2.72E + 06 | 6.00E + 06 | 188.09 | 75.11 | 14.60 |
| | | 1 | 31,965 | 36,814 | 84,417 | 5.19E + 05 | 3.68E + 06 | 1.15E + 07 | 360.93 | 136.67 | 16.25 |
| | 0.5 | 0.1 | 6.82E + 05 | 6.97E + 05 | 8.41E + 05 | 2.17E + 06 | 9.68E + 06 | 2.01E + 07 | 29.50 | 23.92 | 3.17 |
| | | 0.5 | 6.81E + 05 | 6.88E + 05 | 7.51E + 05 | 1.37E + 06 | 6.53E + 06 | 2.81E + 07 | 41.30 | 37.48 | 2.00 |
| | | 1 | 6.82E + 05 | 6.88E + 05 | 7.50E + 05 | 1.36E + 06 | 6.79E + 06 | 3.82E + 07 | 56.06 | 50.98 | 1.99 |
| | 1 | 0.1 | 5.26E + 06 | 5.29E + 06 | 5.53E + 06 | 7.87E + 06 | 2.47E + 07 | 6.29E + 07 | 11.95 | 11.37 | 1.49 |
| | | 0.5 | 5.26E + 06 | 5.27E + 06 | 5.36E + 06 | 6.26E + 06 | 1.45E + 07 | 6.15E + 07 | 11.68 | 11.47 | 1.19 |
| | | 1 | 5.26E + 06 | 5.27E + 06 | 5.35E + 06 | 6.16E + 06 | 1.38E + 07 | 6.80E + 07 | 12.92 | 12.71 | 1.17 |
| | 2 | 0.1 | 4.19E + 07 | 4.19E + 07 | 4.25E + 07 | 4.75E + 07 | 8.99E + 07 | 2.42E + 08 | 5.77 | 5.70 | 1.13 |
| | | 0.5 | 4.19E + 07 | 4.19E + 07 | 4.21E + 07 | 4.37E + 07 | 5.91E + 07 | 1.71E + 08 | 4.07 | 4.05 | 1.04 |
| | | 1 | 4.19E + 07 | 4.19E + 07 | 4.20E + 07 | 4.33E + 07 | 5.56E + 07 | 1.58E + 08 | 3.77 | 3.76 | 1.03 |

observed that as the temperature increases and the polymer goes through glass transition and softens, the tip deflection of the multilayered beam increases. Overall, the analysis shows very good comparison with the experiment, thereby establishing its validity.

## V. Parametric Study Results and Discussion

For the parametric studies in this section, simulations were conducted for a base beam made out of aluminum (Young's modulus, $E_b = 70$ GPa), with a length of 0.3 m, a width of $b = 0.02$ m, and a thickness of $t_b = 0.005$ m. The modulus of the cover layers is $E_c = \alpha_E E_b$, and the thickness of the cover layers is $t_c = \alpha_t t_b$. Similarly, the shear modulus of the polymer layer is $G = \beta_G E_b$ (Poisson's ratio of the polymer is assumed to be 0.435 for calculation of its Young's modulus $E_p$), and the thickness of the polymer layers is $t_p = \beta_t t_b$. As the temperature varies, the shear modulus of the polymer layer can be varied. This corresponds to a variation in the nondimensional parameter $\beta_G$. Changes in effective flexural stiffness for variation in $\beta_G$ are presented for different values and over a wide range of nondimensional system parameters $\alpha_E$ (0.1, 1, 10, and 100), $\alpha_t$ (0.01, 0.05, 0.1, 0.5, 1, and 2), and $\beta_t$ (0.1, 0.5, and 1). Values of $\beta_G$ are considered from $10^{-6}$ to $10^{-1}$.

Results for a clamped–free beam are summarized in Table 1, and results for a pinned–pinned beam are summarized in Table 2. For the clamped–free beam, only the base beam is clamped at the root end. Similarly, for the pinned–pinned beam, only the base beam is pinned at the ends. In addition to the effective flexural stiffness [calculated using Eq. (10a) for clamped–free and using Eq. (10b) for pinned–pinned configurations], ratios of flexural stiffness for a change in $\beta_G$ are also presented in Tables 1 and 2 (in the last 3 columns). The ratio $K_{\max}/K_{\min}$ represents the ratio of the effective flexural stiffness corresponding to the maximum and minimum values of $\beta_G$ considered. However, it should be noted that the maximum value considered ($10^{-1}$) and the minimum value ($10^{-6}$) are 5 orders of magnitude apart: much greater than the change in the polymer-layer modulus that could typically be achieved due to a change in temperature through glass transition. Typically, a change in the polymer modulus of up to 2–3 orders of magnitude is achievable by varying temperature through glass transition. The last two columns in the tables present changes in effective flexural stiffness for change in $\beta_G$ of 3 orders of magnitude. The ratio $K_{\max}/K_{\max-3}$ represents the flexural stiffness change when $\beta_G$ reduces from the maximum value of $10^{-1}$ by 3 orders of magnitude to $10^{-4}$ (corresponding to a relatively stiff polymer heated through glass transition), and the ratio $K_{\min+3}/K_{\min}$ represents flexural stiffness change when $\beta_G$ reduces from $10^{-3}$ by 3 orders of magnitude to a minimum value of $10^{-6}$ (corresponding to a relatively soft polymer heated through glass transition).

Results in Tables 1 and 2 are presented for a wide range of parameter variations. The results for $\alpha_E = 0.1$ (modulus of the cover

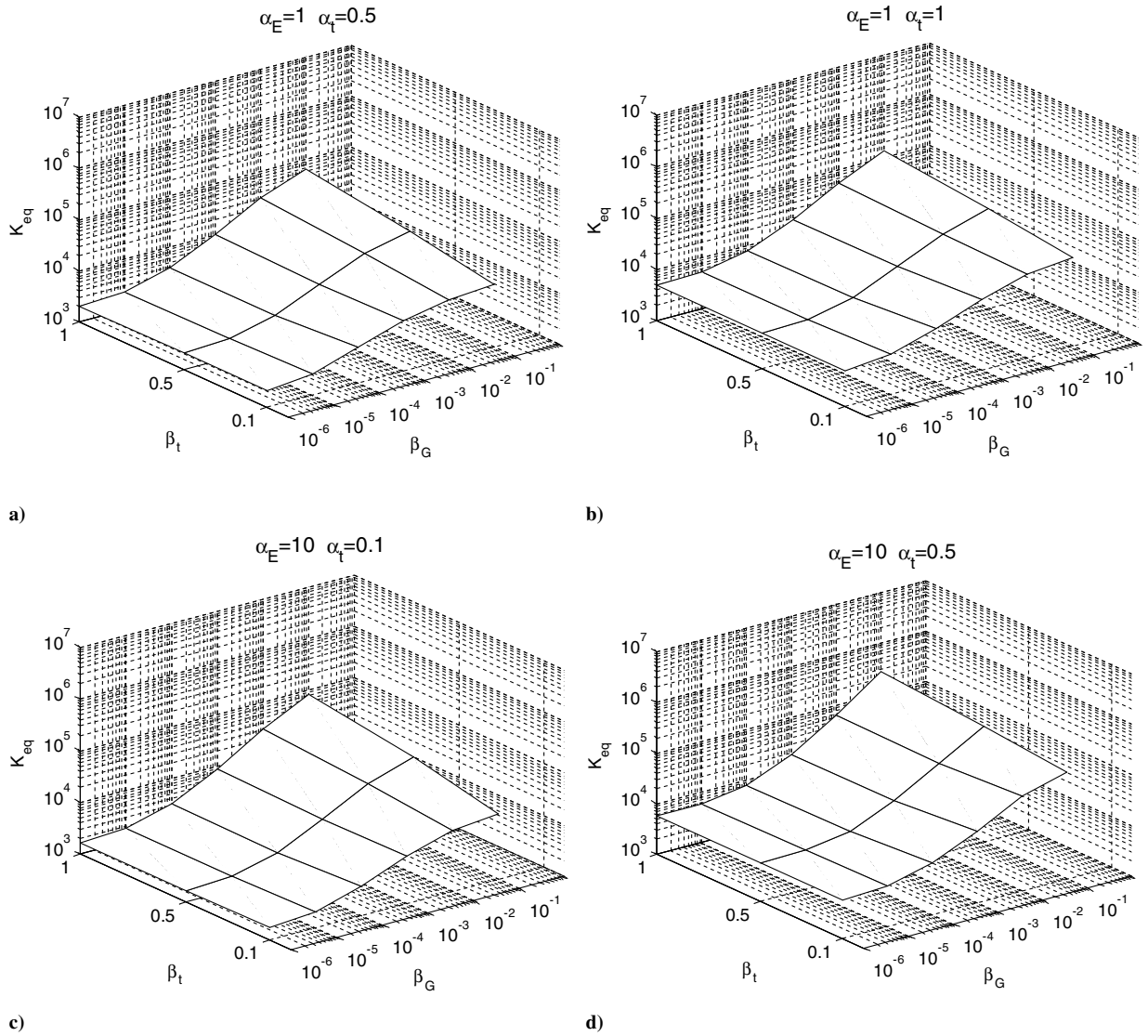


**Fig. 7 Clamped–free beam effective flexural stiffness variation as a function of polymer-layer thickness $\beta_t$ and shear modulus $\beta_G$ for different cover-layer properties.**

layer 1/10th the modulus of the base beam) are of least interest because, intuitively, the change in flexural bending stiffness with such a compliant cover layer would be smallest. This is borne out by the results in the table (relative to stiffness variations observed with higher values of $\alpha_E$). The results are retained in the tables for completeness but are not discussed in the subsequent paragraphs.

From the results in Table 1 for the clamped–free beam, it is observed that if the polymer is relatively stiff and undergoes a modulus reduction of 3 orders of magnitude ($\beta_G$ going from $\beta_{G,\max}$ of $10^{-1}$ to $10^{-4}$), it is possible to realize a change in effective flexural stiffness of around 16–17 (for $\alpha_E = 1$, the cover-layer modulus is equal to the base-beam modulus), 26–33 (for $\alpha_E = 10$, the cover-layer modulus is 10 times greater than the base-beam modulus), and 62–72 (for $\alpha_E = 100$, the cover-layer modulus is 100 times greater than the base-beam modulus). As $\alpha_E$ increases (from 1 to 10 to 100), the $\alpha_t$ values required to realize the largest flexural stiffness variation decrease. This implies that as the cover-layer modulus is increased, its thickness can be reduced. For $\alpha_E = 1$, the largest flexural stiffness variations (of 16–17 for the 3-order-of-magnitude change in $\beta_G$) are observed for $\alpha_t$ of 0.5–1, which is a cover-layer thickness of 50–100% of the base-beam thickness. However, for $\alpha_E = 10$, the largest flexural stiffness variations (of 26–33 for the 3-order-of-magnitude change in $\beta_G$) are observed for $\alpha_t$ of 0.1–0.5, which is a cover-layer thickness of 10–50% of the base-beam thickness, and for $\alpha_E = 100$, the largest flexural stiffness variations (of 62–72 for the 3-order-of-magnitude change in $\beta_G$) are observed for $\alpha_t$ of 0.05–0.1, which is a cover-layer thickness of 5–10% of the base-beam thickness. Irrespective of the values of $\alpha_E$ (1, 10, or 100) and $\alpha_t$ (0.05, 0.1, 0.5, or 1), larger flexural stiffness change is always observed when $\beta_t$ is greatest (corresponding to a value of 1, as compared with values of 0.5 or 0.1, among those considered). Thus, a thicker polymer layer is preferable.

If the polymer is relatively soft and undergoes a modulus reduction of 3 orders of magnitude ($\beta_G$ going from $10^{-3}$ to $\beta_{G,\min}$ of $10^{-6}$), the change in effective flexural stiffness is much smaller. From Table 1, it is observed that the change in flexural stiffness is less than 5 for $\alpha_E = 1$ (compared with 16–17 for the stiffer polymer), just over 5 for $\alpha_E = 10$ (compared with 26–33 for the stiffer polymer), and no greater than 6.4 for $\alpha_E = 100$ (compared with 62–72 for the stiffer polymer). Additionally, it is observed that for any given value of $\alpha_E$, the optimal cover-layer thickness (for the largest change in flexural stiffness) is generally smaller for a softer polymer. From Table 1, it is seen that for $\alpha_E = 1$, the largest flexural stiffness change is obtained for a cover-layer thickness that is 50% of the base-beam thickness ($\alpha_t = 0.5$), compared with a cover-layer thickness ranging from 50–100% of the base-beam thickness for the stiffer polymer. Similarly, for $\alpha_E = 10$, the largest flexural stiffness change is obtained for a cover-layer thickness that is 10% of the base-beam thickness ($\alpha_t = 0.1$), compared with a cover-layer thickness ranging from 10–50% of the base-beam thickness for the stiffer polymer. For

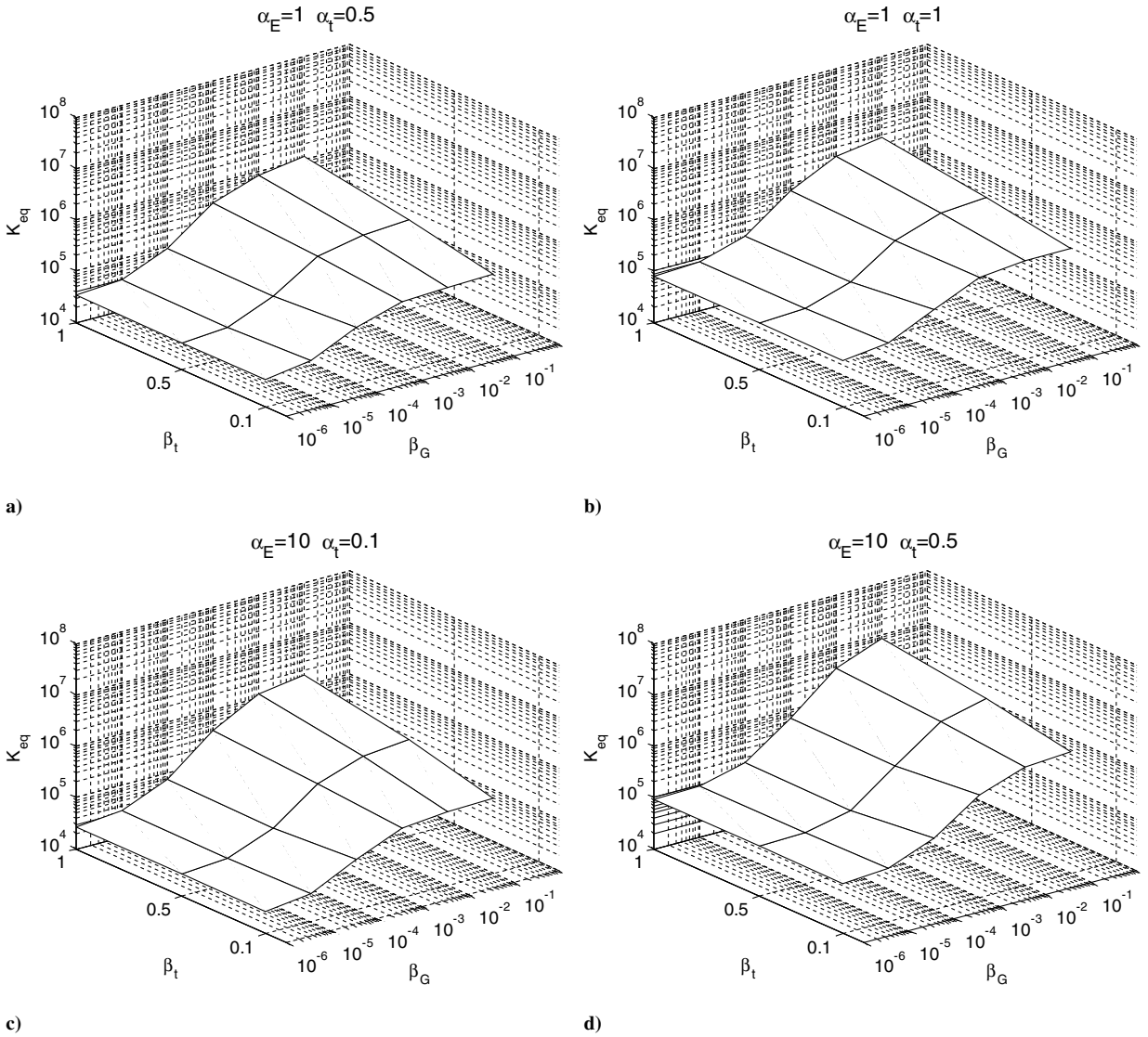


**Fig. 8 Pinned–pinned beam effective flexural stiffness variation as a function of polymer-layer thickness $\beta_t$ and shear modulus $\beta_G$ for different cover-layer properties.**

$\alpha_E = 100$, the largest flexural stiffness change is obtained for a cover-layer thickness that is 5–10% of the base-beam thickness ($\alpha_t = 0.05$–$0.1$), the same as that for the stiffer polymer, but in this case, a lower polymer-layer thickness is preferable ($\beta_t = 0.1$), as opposed to a higher polymer-layer thickness ($\beta_t = 1$), which is favored for the stiffer polymer.

Figures 7a–7d show a graphical representation of the effective flexural stiffness as a function of polymer-layer thickness $\beta_t$ and shear modulus $\beta_G$ for a selection of cover-layer parameter values. Figures 7a and 7b correspond to $\alpha_E = 1$ (cover-layer modulus the same as the base-beam modulus) and $\alpha_t$ values of 0.5 and 1, respectively (which showed the largest change in $K_{\text{eq}}$ for $\alpha_E = 1$). Figures 7c and 7d correspond to $\alpha_E = 10$ (cover-layer modulus that is 10 times the base-beam modulus) and $\alpha_t$ values of 0.1 and 0.5, respectively (which showed the largest change in $K_{\text{eq}}$ for $\alpha_E = 10$). Similar plots for $\alpha_E = 100$ are not presented, because a cover-layer modulus 100 times greater than the base-beam modulus is less realistic (unless the base beam itself is very soft).

Results for a pinned–pinned beam are presented in Table 2. For a relatively stiff polymer undergoing a modulus reduction of 3 orders of magnitude ($\beta_G$ going from $\beta_{G,\max}$ of $10^{-1}$ to $10^{-4}$), it is possible to realize a change in effective flexural stiffness of around 12–16 (for $\alpha_E = 1$, the cover-layer modulus is equal to the base-beam modulus), around 53 (for $\alpha_E = 10$), and 83–137 (for $\alpha_E = 100$). These are somewhat higher than the corresponding changes for the clamped–free case. As $\alpha_E$ increases (from 1 to 10 to 100), the preferred $\alpha_t$ values (which yield the largest flexural stiffness changes) decrease. For $\alpha_E = 1$, the largest flexural stiffness variations are observed for $\alpha_t$ of 0.5–1, which is a cover-layer thickness of 50–100% of the base-beam thickness; for $\alpha_E = 10$, the best $\alpha_t$ is 0.5; and for $\alpha_E = 100$, the best $\alpha_t$ ranges from 0.05–0.1. This observation that the cover-layer thickness can be reduced as its modulus is increased is similar to that for the clamped–free beam. As with the clamped–free case, the largest flexural stiffness change is always observed when $\beta_t$ is greatest (corresponding to a value of 1, as compared with values of 0.5 or 0.1, among those considered, irrespective of the value of $\alpha_E$ or $\alpha_t$).

As with the clamped–free case, the possible change in effective flexural stiffness for a softer polymer undergoing a modulus reduction of 3 orders of magnitude ($\beta_G$ going from $10^{-3}$ to $\beta_{G,\min}$ of $10^{-6}$) is also examined. Table 2 shows possible changes in flexural stiffness of around 12.4 for $\alpha_E = 1$ (compared with a change of less than 5 for the clamped–free beam), around 14.8 for $\alpha_E = 10$ (compared with a change of just over 5 for the clamped–free case), and around 21 for $\alpha_E = 100$ (compared with a change of up to 6.4 for the clamped–free case). With a relatively soft polymer, the possible changes in effective flexural stiffness are clearly significantly larger for the pinned–pinned beam than with the clamped–free beam. Other observations are generally similar to the clamped–free case, with changes in flexural stiffness smaller than those possible with a stiffer polymer, preferred cover-layer thickness generally smaller for a softer polymer for $\alpha_E$ values of 1 and 10, and preferred polymer-layer thickness reducing (from $\beta_t = 1$ for $\alpha_E$ values of 1 and 10) to smaller values ($\beta_t = 0.1$) for $\alpha_E = 100$.

Figures 8a–8d show a graphical representation of the effective flexural stiffness as a function of polymer-layer thickness $\beta_t$ and shear modulus $\beta_G$ for a selection of cover-layer parameter values. Figures 8a and 8b correspond to $\alpha_E = 1$ (cover-layer modulus the same as the base-beam modulus) and $\alpha_t$ values of 0.5 and 1, respectively (which showed the largest change in $K_{\text{eq}}$ for $\alpha_E = 1$). Figures 8c and 8d correspond to $\alpha_E = 10$ (cover-layer modulus that is 10 times the base-beam modulus) and $\alpha_t$ values of 0.1 and 0.5, respectively (which showed the largest change in $K_{\text{eq}}$ for $\alpha_E = 10$).

## VI. Conclusions

The ability to modulate the flexural bending stiffness of a multilayer beam is examined in this paper. The multilayered beam comprises a base layer with polymer layers on the upper and lower surfaces and stiff cover layers. A change in flexural bending stiffness of the beam is achieved by varying the shear modulus of the polymer layers, which can be accomplished by heating the polymer through glass transition A high polymer modulus couples the stiff cover layers to the base beam, resulting in high overall flexural bending stiffness. A reduction in the polymer modulus results in shear deformation in the polymer layer and decoupling of the stiff cover layers from the base beam. This results in a reduction of the flexural bending stiffness.

A finite element analysis is developed for the multilayered beam and its validity is verified experimentally. In the experiment, the polymer layers are each divided into two sublayers and an electric heating pad is embedded between. This is used to control the temperature of the polymer layer. The measured and predicted tip-displacement increases of a clamped–free beam show good agreement as the temperature of the polymer layer is increased (and its modulus is reduced).

The finite element analysis is then used to conduct a parametric study and identify design features that will enable the largest change in flexural bending stiffness with a finite change in the polymer-layer modulus (of up to 3 orders of magnitude, which is typical of many polymers undergoing glass transition). To achieve the largest change in the flexural bending stiffness, the following observations could be drawn from the parametric studies:

1) The highest possible cover-layer modulus is always preferred.

2) As the cover-layer modulus increases, its required thickness decreases.

3) In general, stiffer polymers are preferred (compared with polymers that are more compliant at low temperature in the glassy state, undergoing the same reduction in shear modulus through glass transition).

4) A higher polymer-layer thickness is generally preferred. The only exception appeared to be the case when the polymer has a relatively low shear modulus and the cover-layer modulus is very high. In that case, a slightly larger change in flexural bending stiffness was observed when the polymer layer was thinner.

5) For the best design parameters (within the range considered), a change in flexural bending stiffness by a factor of over 70 for a clamped–free beam and by a factor of over 130 for a pinned–pinned beam was predicted.

## References

[1] Kobori, T., Takahashi, M., Nasu, T., Niwa, N., and Ogasawara, N., "Seismic Response Controlled Structure with Active Variable Stiffness System," *Earthquake Engineering & Structural Dynamics*, Vol. 22, No. 11, Nov. 1993, pp. 925–941. doi:10.1002/eqe.4290221102

[2] Takahashi, M., Kobori, T., Nasu, T., Niwa, N., and Kurata, N., "Active Response Control of Buildings for Large Earthquakes—Seismic Response Control System with Variable Structural Characteristics," *Smart Materials and Structures*, Vol. 7, No. 4, 1998, pp. 522–529. doi:10.1088/0964-1726/7/4/012

[3] Sahasrabudhe, S., and Nagarajaiah, S., "Effectiveness of Variable Stiffness Systems in Base-Isolated Bridges Subjected to Near-Fault Earthquakes: An Experimental and Analytical Study," *Journal of Intelligent Material Systems and Structures*, Vol. 16, No. 4, Sept. 2005, pp. 743–756. doi:10.1177/1045389X05054999

[4] Onoda, J., Endo, T., Tamaoki, H., and Watanabe, N., "Vibration Suppression by Variable-Stiffness Members," *AIAA Journal*, Vol. 29, No. 6, June 1991, pp. 977–983. doi:10.2514/3.59943

[5] Yong, C., Zimcik, D. G., Wickramasinghe, V. K., and Nitzsche, F., "Development of the Smart Spring for Active Vibration Control of Helicopter Blades," *Journal of Intelligent Material Systems and Structures*, Vol. 15, No. 1, Jan. 2004, pp. 37–47. doi:10.1177/1045389X04039655

[6] Davis, C. L., and Lesieutre, G. A., "An Actively Tuned Solid-State Vibration Absorber Using Capacitive Shunting of Piezoelectric Stiffness," *Journal of Sound and Vibration*, Vol. 232, No. 3, 2000, pp. 601–617. doi:10.1006/jsvi.1999.2755

[7] Clark, W. W., "Vibration Control with State-Switched Piezoelectric Materials," *Journal of Intelligent Material Systems and Structures*, Vol. 11, No. 4, 2000, pp. 263–271. doi:10.1106/18CE-77K4-DYMG-RKBB

[8] Corr, L. R., and Clark, W. W., "Comparison of Low-Frequency Piezoelectric Switching Shunt Techniques for Structural Damping," *Smart Materials and Structures*, Vol. 11, No. 3, 2002, pp. 370–376. doi:10.1088/0964-1726/11/3/307

[9] Otsuka, K., and Wayman, C. M., *Shape Memory Materials*, 1st ed., Cambridge Univ. Press, New York, 1998, pp. 203–219.

[10] Hodgson, D. E., *Using Shape Memory Alloys*, Shape Memory Applications, Inc., Sunnyvale, CA, 1988.

[11] Wei, Z. G., Sandstrom, R., and Miyazaki, S., "Review: Shape-Memory Materials and Hybrid Composites for Smart Systems," *Journal of Materials Science*, Vol. 33, No. 15, 1998, pp. 3743–3762. doi:10.1023/A:1004692329247

[12] Lendlein, A., and Kelch, S., "Shape-Memory Polymers," *Angewandte Chemie*, Vol. 41, Verlag Chemie, Weinheim, Germany, 2002, pp. 2034–2057.

[13] Atli, B., Gandhi, F., and Karst, G., "Thermomechanical Characterization of Shape Memory Polymers," *Electroactive Polymers and Devices (EAPD) 2007*, edited by Y. Bar-Cohen, Proceedings of the SPIE, Vol. 6524, Society of Photo-Optical Instrumentation Engineers, Bellingham, WA, 2007, Paper 65241S.

[14] Ginder, J. M., Nichols, M. E., Elie, L. D., and Clark, S. M., "Controllable-Stiffness Component Based on Magnetorheological Elastomers," *Smart Structures and Materials 2000: Smart Structures and Integrated Systems*, edited by N. M. Wereley, Proceedings of SPIE, Vol. 3985, Society of Photo-Optical Instrumentation Engineers, Bellingham, WA, 2000, pp. 418–425.

[15] Perkins, D. A., Reed, J. L., Jr., and Havens, Ernie, "Adaptive Wing Structures," *Smart Structures and Materials 2004: Industrial and Commercial Applications of Smart Structures Technologies*, edited by E. H. Anderson, Proceedings of SPIE, Vol. 5388, Society of Photo-Optical Instrumentation Engineers, Bellingham, WA, 2004, pp. 225–233.

[16] Reed, J. L., Jr., Hemmelgarn, C. D., Pelley, B. M., and Havens, Ernie, "Adaptive Wing Structures," *Smart Structures and Materials 2005: Industrial and Commercial Applications of Smart Structures Technologies*, Edited by E. V. White, Proceedings of the SPIE, Vol. 5762, Society of Photo-Optical Instrumentation Engineers, Bellingham, WA, 2005, pp. 132–142.

[17] Hodigere-Siddaramaiah, V., and Cooper, J. E., "On the Use of Adaptive Internal Structures to Optimise Wing Aerodynamic Distribution," 47th AIAA/ASME/ASCE/AHS/ASC Structures, Structural Dynamics, and Materials Conference, Newport, Rhode Island, AIAA Paper 2006-2131, May 2006.

[18] McKnight, G., and Henry, C., "Variable Stiffness Materials for Reconfigurable Surface Applications," *Smart Structures and Materials 2005: Active Materials: Behavior and Mechanics*, edited by W. D. Armstrong, Proceedings of the SPIE, Vol. 5761, Society of Photo-Optical Instrumentation Engineers, Bellingham, WA, 2005, pp. 119–126.

[19] Gandhi, F., and Kang, S.-G., "Beams with Controllable Flexural Stiffness," *Smart Materials and Structures*, Vol. 16, No. 4, Aug. 2007, pp. 1179–1184. doi:10.1088/0964-1726/16/4/028

[20] Gandhi, F., "Influence of Nonlinear Viscoelastic Material Characterization on Performance of Constrained Layer Damping Treatment," *AIAA Journal*, Vol. 39, No. 5, May 2001, pp. 924–931. doi:10.2514/2.1397

[21] Gandhi, F., and Munsky, B., "Effectiveness of Active Constrained Layer Damping Treatments in Attenuating Resonant Oscillations," *Journal of Vibration and Control*, Vol. 8, No. 6, 2002, pp. 747–775.

[22] Gandhi, F., and Munsky, B., "Comparison of Damping Augmentation Mechanisms with Position and Velocity Feedback in Active Constrained Layer Treatments," *Journal of Intelligent Material Systems and Structures*, Vol. 13, No. 5, May 2002, pp. 317–326. doi:10.1177/104538902761696788

[23] Gandhi, F., Remillat, C., Tomlinson, G., and Austruy, J., "Constrained Layer Damping with Gradient Viscoelastic Polymers for Effectiveness over Broad Temperature Range," *AIAA Journal*, Vol. 45, No. 8, Aug. 2007, pp. 1885–1893. doi:10.2514/1.19574

[24] Baz, A., and Ro, J., "Optimum Design and Control of Active Constrained Layer Damping," *Journal of Mechanical Design*, Vol. 117, No. B, June 1995, pp. 135–144. doi:10.1115/1.2836447

[25] Baz, A., "Optimization of Energy Dissipation Characteristics of Active Constrained Layer Damping," *Smart Materials and Structures*, Vol. 6, No. 3, 1997, pp. 360–368.

[26] Shen, I. Y., "Hybrid Damping Through Intelligent Constrained Layer Treatments," *Journal of Vibration and Acoustics*, Vol. 116, No. 3, July 1994, pp. 341–349. doi:10.1115/1.2930434

[27] Shen, I. Y., "Bending-Vibration Control of Composite and Isotropic Plates Through Intelligent Constrained Layer Treatments," *Smart Materials and Structures*, Vol. 3, No. 1, 1994, pp. 59–70. doi:10.1088/0964-1726/3/1/008

[28] Azvine, B., Tomlinson, G. R., and Wynne, R. J., "Use of Active Constrained-Layer Damping for Controlling Resonant Vibration," *Smart Materials and Structures*, Vol. 4, No. 1, 1995, pp. 1–6. doi:10.1088/0964-1726/4/1/001

[29] Huang, S. C., Inman, D. J., and Austin, E. M., "Some Design Considerations for Active and Passive Constrained Layer Damping Treatments," *Smart Materials and Structures*, Vol. 5, No. 3, 1996, pp. 301–313. doi:10.1088/0964-1726/5/3/008

[30] Wang, G., and Wereley, N. M., "Spectral Finite Element Analysis of Sandwiched Beams with Passive Constrained Layer Damping," *Journal of Vibration and Acoustics*, Vol. 124, No. 3, pp. 376–386. doi:10.1115/1.1469007, 2002.

[31] Nashif, A. D., Jones, D. I. G., and Henderson, J. P., *Vibration Damping*, Wiley, Hoboken, NJ, 1985.

J. Samareh
*Associate Editor*